CMS Draft Analysis Note

The content of this note is intended for CMS internal use and distribution only

2015/01/22
Head Id: 268258
Archive Id: 274622
Archive Date: 2014/11/18
Archive Tag: trunk

Search for a neutral pseudo-scalar Higgs boson decaying to a Z boson and an SM-like Higgs boson using tau final states

C. Caillol[1], B. Clerbaux[1], S. Cooperstein[2], S. Dasu[3], A. Mohammadi[1], I. Ojalvo[3], T. Ruggles[3], and T. Sarangi[3]

[1] IIHE-ULB, Université Libre de Bruxelles, Brussels, Belgium
[2] Princeton University, U.S.A
[3] University of Wisconsin-Madison, WI 53706, U.S.A.

Abstract

Results of a search for a neutral pseudo-scalar Higgs boson (A) decaying to a Z boson and an SM-like Higgs boson (h) in the pp collision data recorded by CMS in 2012 are presented. The analysis targets final states where the SM-like Higgs boson decays to a pair of tau leptons, and the Z boson to a pair of light leptons. The search is performed in the context of the minimal supersymmetric extension of the standard model. The dataset corresponds to an integrated luminosity of 19.7 fb^{-1} recorded at 8 TeV center-of-mass energy. No excess is found and upper limits at 95% confidence limit are set on the A production cross-section in the mass range $220 < m_A < 350$ GeV.

1 Introduction

In the Yang-Mills theory of weak physics, all the gauge bosons are required to be massless. However, it was clear experimentally that the masses of the weak force mediators ($W^{+/-}$, Z) are on the order of 80 GeV. The process of electroweak symmetry breaking was proposed in order to provide mass to the weak force mediators. This theory introduces a new complex doublet. Through the process of spontaneous symmetry breaking, the degrees of freedom in this complex doublet are reduced from four to one. This remaining degree of freedom corresponds to a new scalar field with a non-zero vacuum expectation value, the Higgs field. The Higgs field implied the existence of new particle, the Higgs boson, which is an excitation of the Higgs field. However, the mass of the Higgs boson is an unspecified parameter in the theory. Since its proposal, experimental physicists have been searching for evidence of a Higgs boson. Until very recently, however, the particle remained elusive.

On July 4, 2012 the CMS and ATLAS experiments at the LHC confirmed the observation of a standard model Higgs-like boson with a mass of about 125 GeV [1].

Supersymmetry provides an elegant and simple solution to many open questions in particle physics, such as the unification of coupling constants or the hierarchy problem. The supersymmetric model predicts the existence of a bosonic superpartner for each standard model fermion and a fermionic superpartner for each standard model boson. This new symmetry of nature effectively doubles the number of particles in the universe. If this symmetry were unbroken, each standard model particle would have a superpartner with the same mass. If this were the case, however, supersymmetric particles would have been discovered long ago. It is therefore necessary that supersymmetry is a broken symmetry. Unfortunately, this makes the masses of the supersymmetric particles unspecified. There are compelling arguments, however, that suggest that the lightest supersymmetric particles should have masses on the 1 TeV scale [2]. For this reason, many physicists expect to experimentally observe signs of supersymmetric particles during LHC runs.

The most basic extension of the standard model that includes supersymmetry is the Minimal Supersymmetric Standard Model (MSSM). MSSM requires the existence of two complex scalar Higgs fields. This leads to two neutral CP-even Higgs particles, h and H, a CP-odd Higgs particle A, and two charged and CP-even Higgs particles, H^+ and H^-. The masses of these five Higgs particles can be specified by two independent parameters, the mass of the A and tanβ, defined as:

$$tan\beta = v_1/v_2 \tag{1}$$

where v_1 and v_2 are the vacuum expectation values for the neutral component of the Higgs field which couples to up and down quarks, respectively [2]. MSSM predicts that the decay of the A into a Z boson and h has a relatively high branching fraction in the mass range between 260 GeV and 340 GeV. For an A mass less than 260 GeV, the A predominately decays to neutralinos. For an A mass greater than 340 GeV, A decay is dominated by $t\bar{t}$. Therefore, it is convenient to probe this mass range using the A $\rightarrow$ Zh mode. A masses between 220 and 350 GeV are probed in this analysis.

The presence of the light leptons orginating from the Z boson helps isolating the signal from standard model backgrounds. The highest sensitivity to A signal is therefore achieved for h final states with large branching ratios. Limits on $A \rightarrow Zh \rightarrow llbb$ have been set in [3]. The present analysis searches for an A which decays to a Z and an h, where the Z boson decays to

e^+e^- or $\mu^+\mu^-$ and the Higgs boson decays to $\tau^+\tau^-$. The methodology of this analysis is very similar to the search for standard model Higgs associated production with a Z boson using tau final states [4].

2 Data and simulations

2.1 Samples

The search is performed using the DoubleElectron and DoubleMuon primary datasets collected by CMS in 2012, at the center-of-mass energy $\sqrt{s} = 8$ TeV. The analysed datasets are detailed in Tab. 1.

The trigger paths used in this analysis are the following:

- Mu17_Mu8
- Mu17_TkMu8
- Ele17_CaloIdT_CaloIsoVL_TrkIdVL_TrkIsoVL_Ele8_CaloIdT_CaloIsoVL_TrkIdVL_TrkIsoVL

Table 1: Collision datasets from 2012 data taking.

Dataset
/DoubleElectron/Run2012A-22Jan2013-v1/AOD
/DoubleElectron/Run2012B-22Jan2013-v1/AOD
/DoubleElectron/Run2012C-22Jan2013-v1/AOD
/DoubleElectron/Run2012D-22Jan2013-v1/AOD
/DoubleMu/Run2012A-22Jan2013-v1/AOD
/DoubleMuParked/Run2012B-22Jan2013-v1/AOD
/DoubleMuParked/Run2012C-22Jan2013-v1/AOD
/DoubleMuParked/Run2012D-22Jan2013-v1/AOD

Signal as well as ZZ diboson production and triboson WZZ, WWZ and ZZZ production, are generated with MADGRAPH [5]. The τ–lepton decays are simulated with TAUOLA [6], which includes spin effects. Table 2 shows the MC samples and their cross section times branching ratios production for signal and backgrounds. Signal cross-sections at different masses are not mentioned in this table, because the results presented in this note focus on a model-independent search, and because, in the MSSM, cross-sections also depend on $\tan\beta$. However, Fig. 1 illustrates the A production cross-section in gluon fusion and associated production, as well as $A \to Zh$ branching ratio predicted by FeynHiggs in the m_h^{max} MSSM scenario.

Minimum bias events generated by PYTHIA are added to all generated Monte Carlo samples according to the "S10" pile-up profile described in [7], using the tools described in [8]. The pile-up expected in data is computed based on instantaneous luminosity and the pp inelastic cross-section. Simulated events are passed through the full GEANT [9] based simulation of the CMS apparatus and are reconstructed using the same version of the CMS event reconstruction software as the data.

2.2 Comparison between Pythia and MadGraph signal samples

MadGraph signal samples have been used in this analysis, but Pythia samples have also been generated. It can be brought out that the Z spin is not correctly handled by Pythia, which results in a non-defined polarization state. This difference affects variables such as $\cos\theta_1$, the

Table 2: Simulation samples for signal (top) and backgrounds (bottom). Signal masses range from 220 to 350 GeV.

Dataset	Cross section
`AToZhToLLTauTau_MA-XXX_Mh1-125_8TeV-madgraph5-pythia6`	x
`ZZJetsTo4L TuneZ2star 8TeV-madgraph-tauola`	0.187
`GluGluToZZTo2L2L_8TeV-gg2zz-pythia6`	0.01203
`TTZJets_8TeV-madgraph_v2`	0.208
`WH_ZH_TTH_HToWW_M-125_lepdecay_8TeV-pythia6`	0.006503
`ZH_HToTauTau_M-125_lepdecay_8TeV-pythia6-tauola`	0.002651
`WWZNoGstarJets_8TeV-madgraph`	0.05795
`WZZNoGstarJets_8TeV-madgraph`	0.01968
`ZZZNoGstarJets_8TeV-madgraph`	0.005527

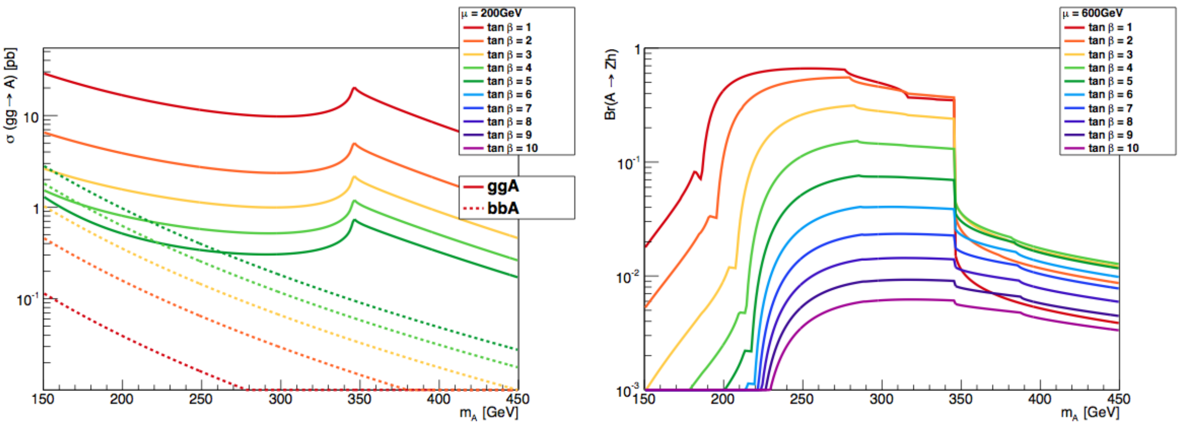

Figure 1: A production cross-section in gluon fusion (solid lines) and associated production (dotted), as well as the $A \to Zh$ branching ratio predicted by FeynHiggs in the m_h^{max} MSSM scenario. [3]

angle between the negatively charged lepton from the Z and the Z flight direction in the Z rest frame, and the lepton transverse momenta, as shown in Fig. 2. In particular, the p_T of the subleading lepton from the Z is harder when simulated by Madgraph. This results in a higher signal acceptance for MadGraph samples, and a limit exclusion approximately 10% tighter.

2.3 Comparison between Pythia and Madgraph ZZ diboson samples

In order to be consistent with the choice of signal samples, the ZZ diboson sample generated with MadGraph has been used in this analysis. The tau p_T spectra as well as the m_A distribution are very similar with those obtained from the Pythia sample, see Fig. 3, while the normalizations are compatible with each other when a cross-section of 0.187 pb is used for the MadGraph sample and 0.130 pb for the Pythia sample.

3 Particle identification

Electrons, muons, and hadronic taus are selected using the criteria defined in the Standard Model H $\to \tau\tau$ search [4, 10]. These selections have been optimized to obtain the best possible sensitivity for a Standard Model Higgs boson. Since the A decays to a Z boson and a

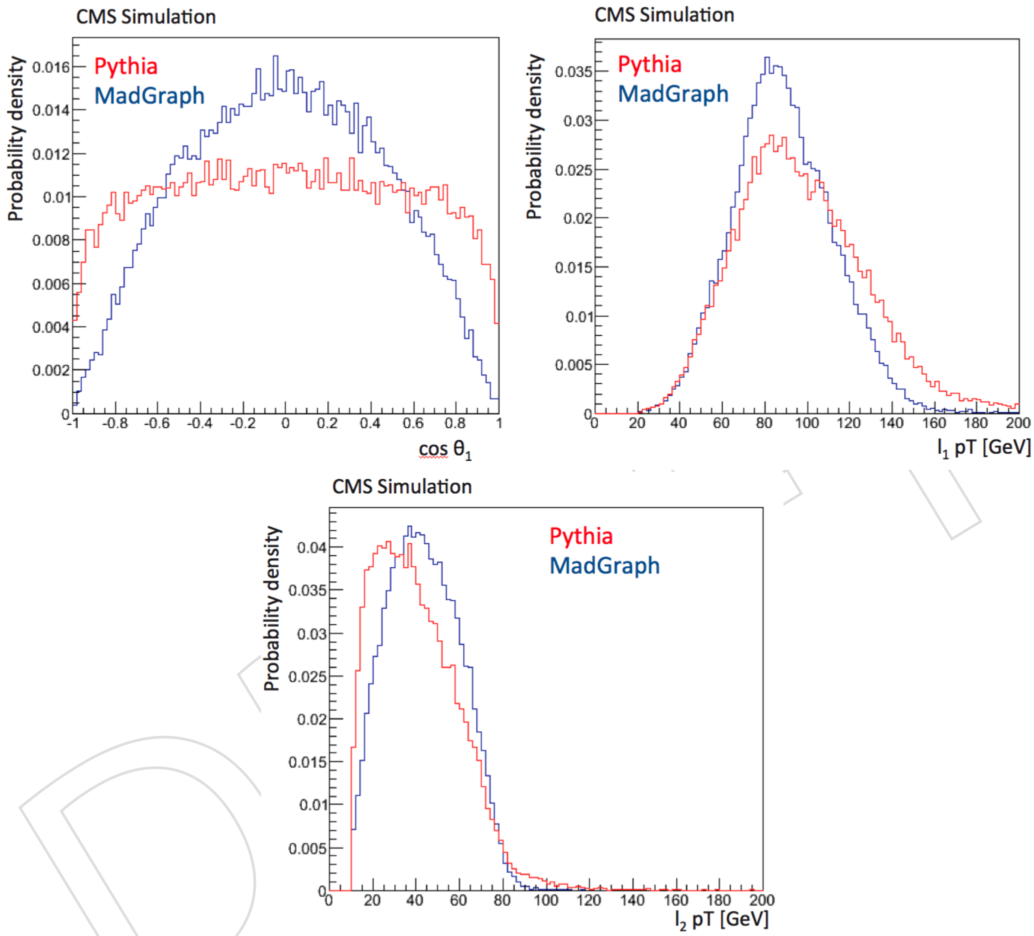

Figure 2: Comparison of the distributions of $\cos\theta_1$, the angle between the negatively charged lepton from the Z and the Z flight direction in the Z rest frame, the leading lepton p_{T} and the subleading lepton p_{T} using Pythia and Madgraph samples. A mass is equal to 350 GeV in these plots.

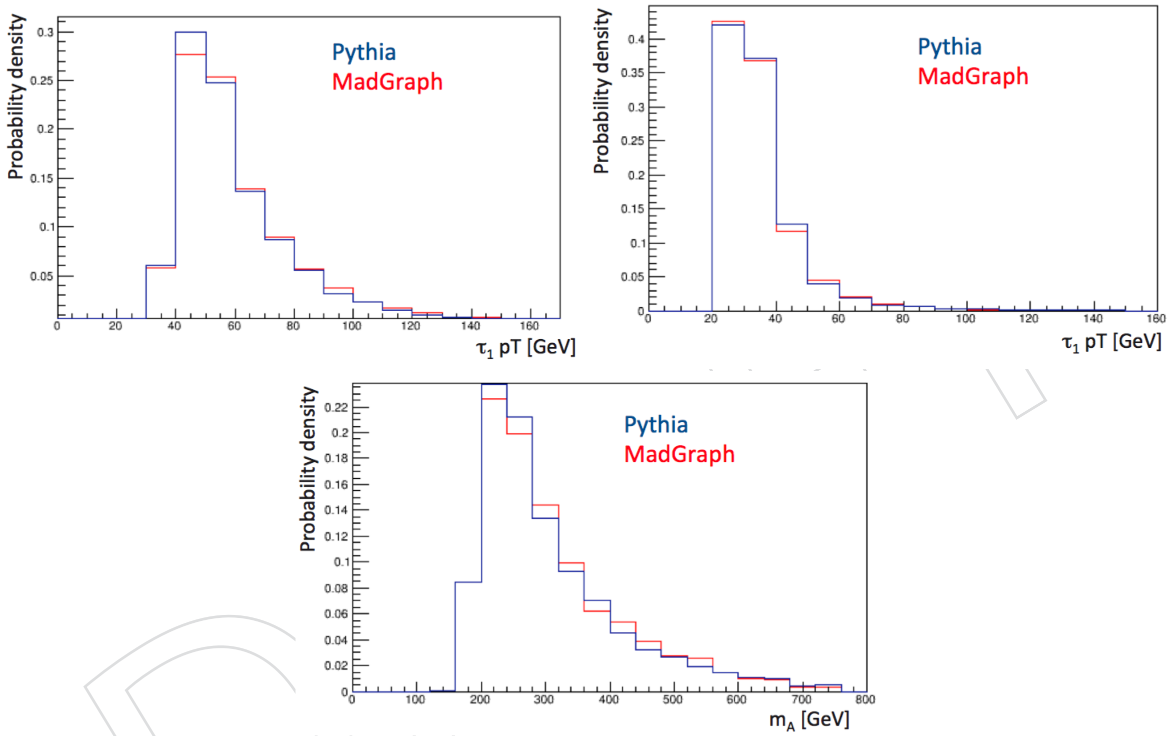

Figure 3: Comparison of the normalized p_T (leading and subleading taus) and m_A spectra for the ZZ diboson samples generated by Pythia and Madgraph. The final state considered here is $\mu\mu\tau_h\tau_h$.

Standard Model-like Higgs boson h, these selections should provide good sensitivity for this MSSM search as well.

3.1 Electron selection

Electron identification uses a Boosted Decision Tree (BDT) discriminator [11]. The BDT is trained with selected data to separate electrons from jets, and takes many kinematic variables as input. For a more complete description of these techniques refer to the relevant references [11].

3.1.1 Very loose electron identification

In addition to the selection criteria used in the inclusive Standard Model H $\rightarrow \tau\tau$ search, this analysis uses a looser electron working point. It is defined in Table 3.

	BDT Discriminator Value (>)		
	$\|\eta\| < 0.8$	$0.8 \leq \|\eta\| < 1.479$	$1.479 \leq \|\eta\|$
$p_T > 10$ GeV	0.50	0.12	0.60

Table 3: Thresholds for the very loose ID BDT discriminator. For an identified electron the discriminator value has to fall above the indicated threshold.

3.1.2 Loose electron identification

In some cases electrons are more selectively identified. These tighter selections, which correspond to the standard electron identification used in the Standard Model Higgs $\rightarrow \tau\tau$ search, are outlined in Table 4.

	BDT Discriminator Value (>)		
	$\|\eta\| < 0.8$	$0.8 \leq \|\eta\| < 1.479$	$1.479 \leq \|\eta\|$
$p_T \leq 20$ GeV	0.925	0.915	0.965
$p_T > 20$ GeV	0.905	0.955	0.975

Table 4: Thresholds for the loose electron ID BDT discriminator. For an identified electron the discriminator value has to fall above the indicated threshold.

3.2 Muon identification

Muons are selected using the particle-flow algorithm detailed in [12].

3.2.1 Loose Muon Identification

"Loose" muons must be identified as 'Global' or 'Tracker' muons via the algorithms outlined in [13].

3.2.2 Tight muon identification

"Tight" muons must pass tight particle-flow selections, as recommended by the 2012 Muon POG [12]:

- Reconstructed as global and PF muons;
- At least one pixel hit associated to the track;
- At least 6 tracker layers with hits;

- At least one hit in the muon system;
- At least two matched segments;
- $\chi^2/N_{DOF} < 10.0$ for global track fit;
- Transverse impact parameter of track reconstructed in pixel plus strip silicon detector $d_{IP} < 2$ mm.

3.3 Light lepton isolation

The relative isolation of electrons and muons is computed with $\Delta\beta$ corrections.

3.4 Hadronic tau identification

Hadronic taus are identified using the ”Hadron Plus Strips” (HPS) algorithm [14, 15]. They are required to pass the decay mode finding discriminator, a specific isolation working point of the Combined 3-Hits isolation, and some light lepton rejections. The exact identification conditions depend on the final state and will be presented in Section **??**.

4 Reconstruction of A mass

The Standard Model H $\rightarrow \tau\tau$ search used a special algorithm (SVFit) to reconstruct the $\tau\tau$ invariant mass. This combines the visible quadri-vectors of the taus, as well as the missing transverse energy and its experimental resolution in a maximum likelihood estimator. For a complete description of this algorithm, refer to [4]. The motivation for using SVFit is that when the taus decay leptonically, they do so through a W boson. This emits a neutrino. SVFit allows for the incorporation of the neutrinos energy into the analysis.

Unlike the Standard Model search, this analysis uses Markov Chain integration to extract the p_T, η, and ϕ of the SV-fitted $\tau\tau$ system in addition to its invariant mass.

The reconstructed A mass is the invariant mass between the Z candidate and the SV–reconstructed h. With respect to using the visible $\tau\tau$ mass, this greatly improves the shape difference between the signal (A $\rightarrow$ Zh) and backgrounds, as well as the signal shape resolution, allowing for better sensitivity. The improvement in limit from reconstructing the h mass with the SVFit algorithm ranges typically from 15 to 20% depending on the final state in this analysis.

A mass shapes for signals are presented in Fig. 4.

5 Event selection

Eight final states are analyzed, according to the decay mode of the Z boson, and to the decay mode of the taus originating from the h boson.

The Z boson consists of a pair of well identified and isolated light leptons (μ or e), which are expected to fire the trigger. The h boson is reconstructed from two taus; leptonic and hadronic decays of taus are considered.

The first step consists in selecting a same-flavour light lepton pair to reconstruct the Z boson, and then identifying the two taus from the h boson.

Details about the event selection follow.

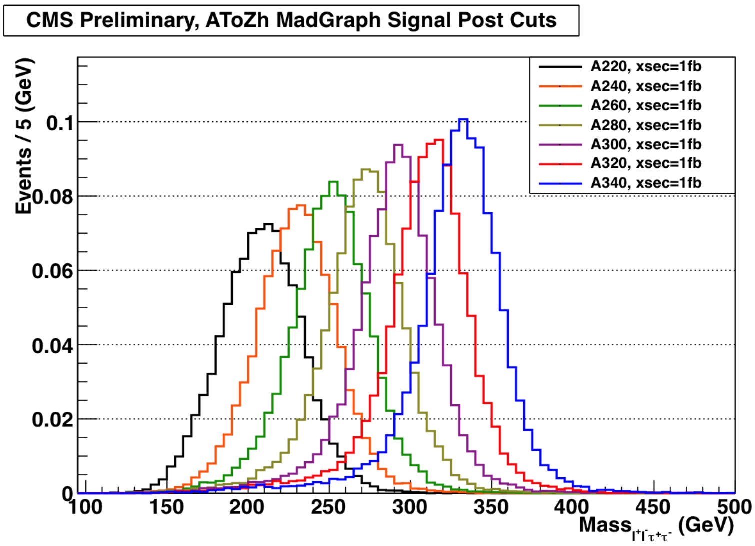

Figure 4: Reconstructed A mass, using the SV-reconstructed h mass. While the distributions are correctly centered on the generated A mass, the resolution is approximately 10% of the generated mass.

5.1 Z boson selection

The Z boson candidate is reconstructed from two same-flavour light leptons of opposite charge, satisfying the criteria described below. If more than one combination of same-flavour light leptons exist, the one with the invariant mass closest to the Z mass is chosen.

$Z \rightarrow \mu^+\mu^-$

The characteristics of the two muons selected to form a Z candidate are:

- Opposite–charge;
- Global and tracker muons passing Particle Flow identification;
- $p_T > 20(10)$ GeV for the leading (subleading) muon, $|\eta| < 2.4$;
- Combined PF Relative Isolation $\Delta\beta$ corrected < 0.30;
- Invariant mass of the two muons between 60 and 120 GeV.

$Z \rightarrow e^+e^-$

The characteristics of the two muons selected to form a Z candidate are:

- Opposite–charge;
- ”Very loose” identification working point;
- $p_T > 20(10)$ GeV/c for the leading (subleading) electron, $|\eta| < 2.5$;
- Not more than one missing inner tracker hit for each electron;
- Combined PF Relative Isolation $\Delta\beta$ corrected < 0.30;
- Invariant mass of the two electrons between 60 and 120 GeV.

5.2 h boson Selection

After having selected two light leptons to form a Z candidate, the h candidate is reconstructed from two additional leptons.

A cut on the scalar pT sum of h legs, $L_{\mathrm{T}}^{\mathrm{h}}$, is applied to lower the reducible background as well as the irreducible background from ZZ diboson production. The thresholds of this cut depend on the final state and have been chosen in such a way as to optimize the sensitivity of the analysis to the presence of an $A \to Zh$ signal for A masses between 220 and 350 GeV.

$h \to \mu\tau_{had}$

In this mode one tau from the h boson decays hadronically while the other decays leptonically to a muon plus neutrinos. The presence of the muon makes this channel relatively clean but small background remains from Z+jets or WZ+jets events, where a Z decays into a pair of electrons or muons, an additional real muon comes from either a b jet or a W boson and, finally, a jet fakes the hadronic τ. The following selection is applied:

- One loosely identified muon with $p_T > 10$ GeV and $|\eta| < 2.4$, passing relative isolation < 0.30;
- One hadronic tau with transverse momentum greater than 21 GeV and $|\eta| < 2.3$, passing "decay mode finding", "against muon 2 tight" and "against electron loose" discriminators, and satisfying the "loose Combined 3 Hits isolation" conditions;
- Charge of the muon and tau must be opposite;
- $L_{\mathrm{T}}^{\mathrm{h}} > 45$ GeV.

$h \to e\tau_{had}$

In this mode one tau from the h boson decays hadronically while the other decays leptonically to an electron plus neutrinos. These channels are expected to have more backgrounds from Z+jets or WZ+jets than the $\mu\tau$ channels since a charged pion or a photon may also fake the electron. The following selection is applied:

- One tightly identified electron with $p_T > 10$ GeV and $|\eta| < 2.5$, with no missing inner tracker hits, and having a relative isolation < 0.3;
- One tau with transverse momentum greater than 21 GeV and $|\eta| < 2.3$, passing "decay mode finding", "against muon 2 loose" and "against electron tight MVA" discriminators, and satisfying the "loose Combined 3 Hits" isolation crieria;
- Charge of the electron and tau must be opposite;
- $L_{\mathrm{T}}^{\mathrm{h}} > 30$ GeV.

$h \to \tau_{had}\tau_{had}$

In this mode both taus from h decay hadronically.

This mode has the largest background due to hadronic jets being reconstructed as taus. The main background source is Z production in association with two or more jets. The following cuts are applied:

- Two opposite–charge τ with $p_T > 21$ GeV and $|\eta| < 2.3$;
- Taus pass "decay mode finding" discriminator, "against muon 2 loose" working point, "against electron loose" working point;
- $L_{\mathrm{T}}^{\mathrm{h}} > 70$ GeV.

$h \to e\mu$

This channel is clean but has the lowest branching ratio in $h \to \tau\tau$ decay. The following cuts are applied:

- One loosely identified muon with $p_T > 10$ GeV and $|\eta| < 2.4$;

- One loosely identified electron with $p_T > 10$ GeV and $|\eta| < 2.5$, with no more than 1 missing inner tracker hit;
- Combined PF Relative Isolation $\Delta\beta$ corrected for muon and electron < 0.30;
- The charge of the electron and the muon must be opposite;
- $L_{\mathrm{T}}^{\mathrm{h}} > 25$ GeV.

5.3 $L_{\mathrm{T}}^{\mathrm{h}}$ cut optimization

$L_{\mathrm{T}}^{\mathrm{h}}$ represents the scalar p_{T} sum of the leptons originating from the h boson. Its distribution significantly differs between the signal and the backgrounds (reducible as well as irreducible) as shown in Fig 6, which permits to increase the $S/\sqrt{B}$ ratio by cutting on it. Special emphasis should be given to optimizing the $L_{\mathrm{T}}^{\mathrm{h}}$ thresholds depending on the h final state. The thresholds minimizing the expected limits at most A masses are chosen. It can be shown, as in Fig 5, that the optimal thresholds are exactly the same as those defined in the SM ZH analysis. This result is expected because of the very similar $L_{\mathrm{T}}^{\mathrm{h}}$ shapes for MSSM $A \to Zh$ and SM ZH processes (Fig. 6). As presented in the paragraphs here-above, $L_{\mathrm{T}}^{\mathrm{h}}$ thresholds of 25, 35, 45 and 70 GeV are chosen in $lle\mu$, $lle\tau_h$, $ll\mu\tau_h$ and $ll\tau_h\tau_h$ final states respectively.

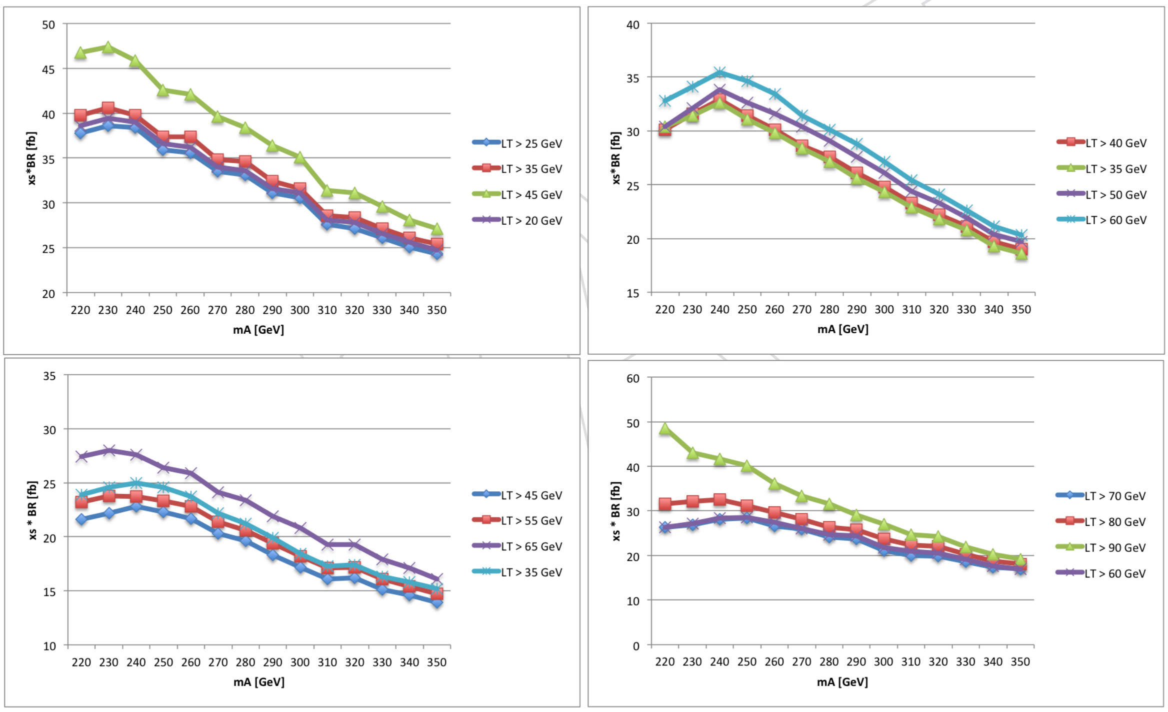

Figure 5: Expected 95% CL limit on the product of the production cross-section and the branching ratio for $A \to Zh \to ll\tau\tau$ as a function of m_A for different $L_{\mathrm{T}}^{\mathrm{h}}$ thresholds, in $lle\mu$ (top left), $lle\tau_h$ (top right), $ll\mu\tau_h$ (bottom left) and $ll\tau_h\tau_h$ final states. The chosen thresholds are respectively 25, 30, 45 and 70 GeV.

5.4 Additional requirements

Some common cuts are applied to all final states. To remove $t\bar{t}$ background, the event should not contain any b-jet with $p_T > 20$ GeV, $|\eta| < 2.4$, bDiscriminator('combinedSecondaryVertexBJetTags') > 0.679. A 1% yield uncertainty due to the b-jet veto is considered (see Sec. 9).

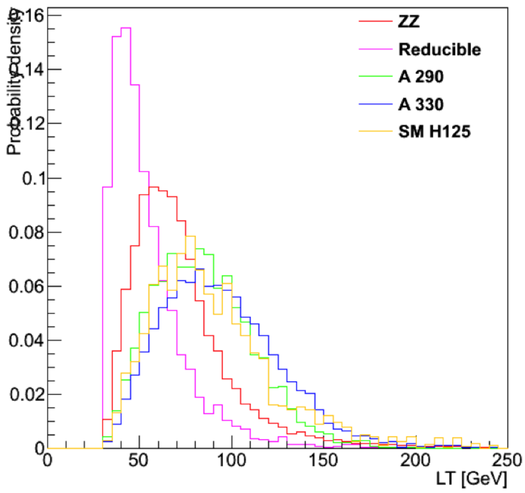

Figure 6: $L_{\mathrm{T}}^{\mathrm{h}}$ normalized distributions for the signal at different A masses, and backgrounds, in the $ll\mu\tau_h$ final state.

Events that contain more well identified and isolated electrons and muons than expected in the considered final state are vetoed. A well-identified and isolated electron is defined as:

- $p_{\mathrm{T}} > 10$ GeV, $|\eta| < 2.5$;
- relative isolation < 0.3;
- very loose MVA electron identification,

while well-identified and isolated muons are defined as:

- $p_{\mathrm{T}} > 10$ GeV, $|\eta| < 2.4$;
- relative isolation < 0.3;
- loose muon identification.

This extra lepton veto ensures that there is no event overlap between the different categories. It may be worth noticing that there is no condition on extra identified and isolated taus in the events.

All four objects are further required to be separated from each other by ΔR larger than 0.5, and to come from the same primary vertex ($\Delta z < 0.1$ cm). Some cleaning conditions are applied to the objects: electrons are required not to overlap with any well identified and isolated muon (as defined above) within $\Delta R < 0.1$, while taus are required not to overlap with any well identified and identified muon or any well identified and isolated electron within $\Delta R < 0.1$. Furthermore, b-jets are also required not to overlap with any well identified and identified muon or any well identified and isolated electron within $\Delta R < 0.4$.

6 Background estimation

Background to A$\rightarrow$ Zh search can be divided into two components that contribute roughly in equal proportions: irreducible and reducible backgrounds. The next paragraphs present how these backgrounds are estimated in the analysis.

6.1 Irreducible background

The predominant source of irreducible background is ZZ diboson production. The process yields exactly the same final states as the expected signal. Both qqZZ and GluGluZZ production modes are taken into account and their contribution are directly estimated from MC (NNLO).

Another significant source of irreducible background in this analysis is SM h associated production with a Z boson. In this process, an off-shell Z radiates a SM h boson. When the Z decays to light leptons and the h decays to $\tau^+\tau^-$, the final states are indistinguishable from signal events. h to WW associated with a Z boson is also considered as an irreducible background; it mainly contributes to $e\mu$ final state. Triboson WWZ/WZZ/ZZZ production is also considered as irreducible background. Finally, ttZ, where one Z decays into an electron or a muon pair, and both top quarks decay leptonically (to e, μ or τ) with an additional b–jet, though small thanks to the b–jet veto, also contributes to the irreducible background. All the processes are regrouped under the "rare" appellation.

6.2 Reducible background

The primary source of reducible background in final states with two hadronic taus is Z+jets, while another significant source is SM WZ+jets production in other final states with three or more light leptons. In $ll\tau_h\tau_h$ final states, the reducible background is essentially composed of Z+jets events with a least two jets, whereas in $lle\tau_h$ and $ll\mu\tau_h$ final states, the main contribution to the reducible background comes from WZ+jets with 3 light leptons, see Fig. 7. In both processes, one or more jets are misidentified as leptons. The contribution from these processes to the final selected events is estimated using a data-driven fake rate scheme.

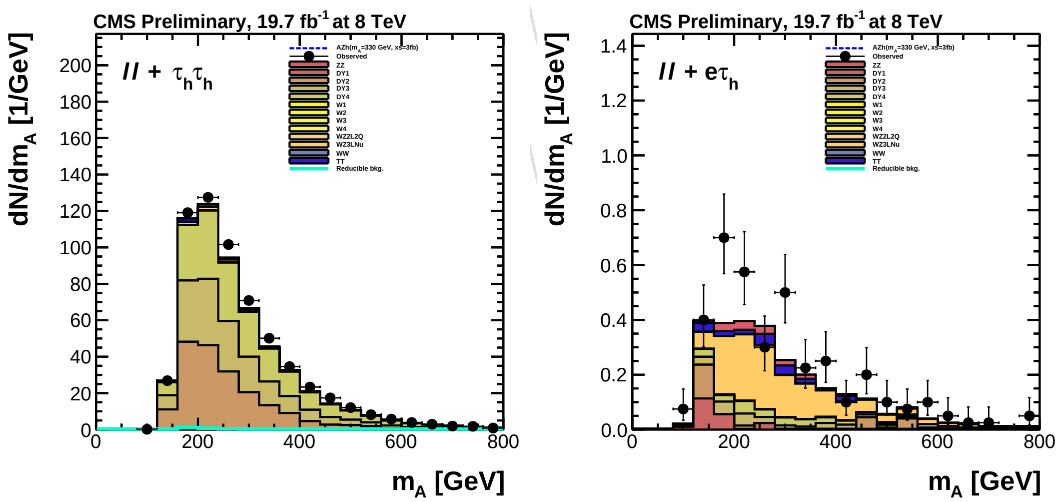

Figure 7: Reducible background composition, from Monte Carlo simulations, in $ll\tau_h\tau_h$ (left) and $lle\tau_h$ (right) final states. The selection is similar as explained in Sec. 5, but the taus have the same sign and are anti-isolated, while there is no cut on their scalar p_T sum.

The probability of a jet faking a lepton, the "fake rate", is measured in a signal–free region. In this region, events are required to pass all the final state selections, except that the reconstructed tau candidates are required to have the same sign. This effectively eliminates any possible signal while maintaining roughly the same proportion of reducible background events.

6.2.1 Jet $\rightarrow e$ and jet $\rightarrow \mu$ fake rates

Electron (muon) fake rates are measured using $e\tau_h$ ($\mu\tau_h$) final states. Electron (muon) candidates are selected as outlined in Section **??** for the $e\tau_h$ ($\mu\tau_h$) final states, with the following exceptions:

- No isolation requirement;
- No identification (Section 3.1.1);
- No cut on the scalar p_T sum;
- Electron (muon) and tau have the same sign;
- Transverse mass between the electron (muon) and the missing transverse energy $<$ 30 GeV to suppress real leptons from WZ and ZZ.

Events that pass these selections define the "denominator" region. Electrons (muons) that also pass the identification and isolation requirements are included in the "numerator" region". The fake rate is calculated as the ratio of the number of events in the numerator region to the number of events in the denominator region. The fake rate is measured for ranging values of the closest jet p_T, then fitted with a falling exponential, as shown in Fig. 8. The best-fit exponential function is used to estimate the fake rate, $F(jet p_T)$ for a given data event.

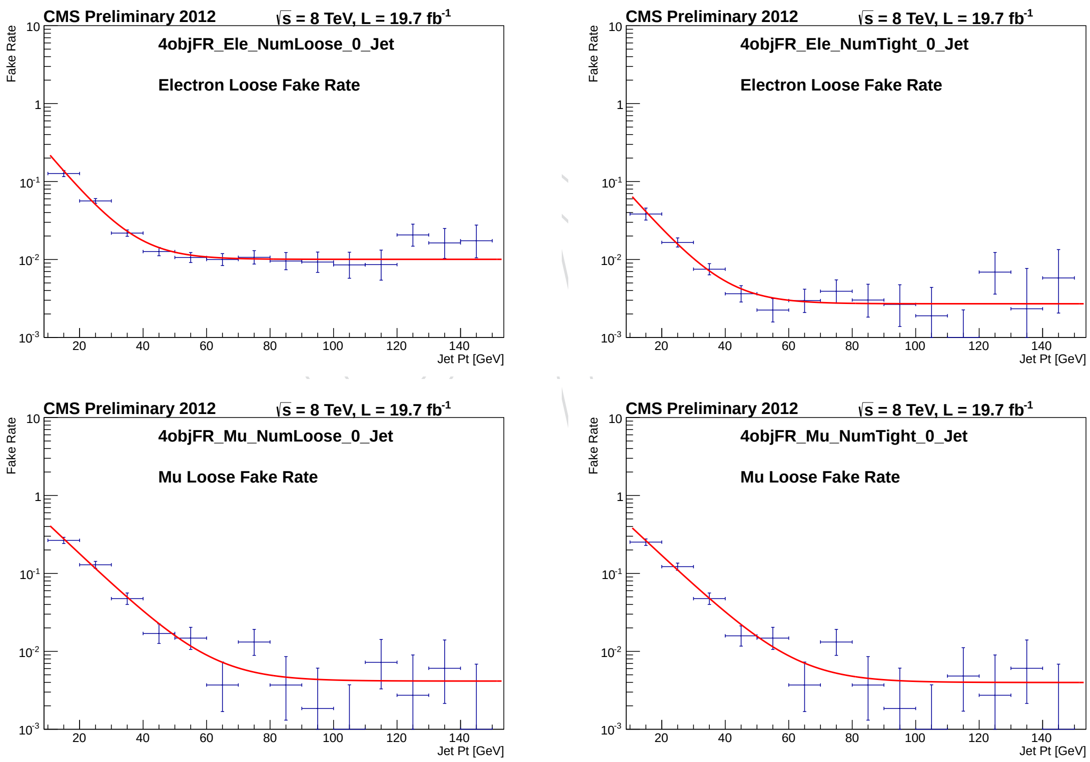

Figure 8: Fit functions for jet $\rightarrow e$ (top) and jet $\rightarrow \mu$ (bottom) fake rates, in the case of loose (left) and tight (right) identification and isolation. The distributions are fitted as a function of the p_{T} of the jet closest to the reconstructed light leptons.

6.2.2 Jet $\rightarrow \tau_{had}$ fake rate measurement in $ll + \tau_h\tau_h$ final states

The hadronic tau fake rate is measured from the $\tau_h\tau_h$ channels. The selections are the same as those outlined in Section **??**, with the exception that the cut on the scalar p_T sum has been reduced to 50 GeV. The fake rate is calculated as the ratio of the number of events that pass all selections to the number of events that pass all selections other than isolation. As is done for electrons and muons, this fake rate is measured for various bins of closest jet p_T, then fitted with a falling exponential. Two fits are performed, depending on whether the tau is reconstructed in the barrel ($|\eta| < 1.4$) or endcap ($|\eta| > 1.4$) of the detector, see Fig. 9.

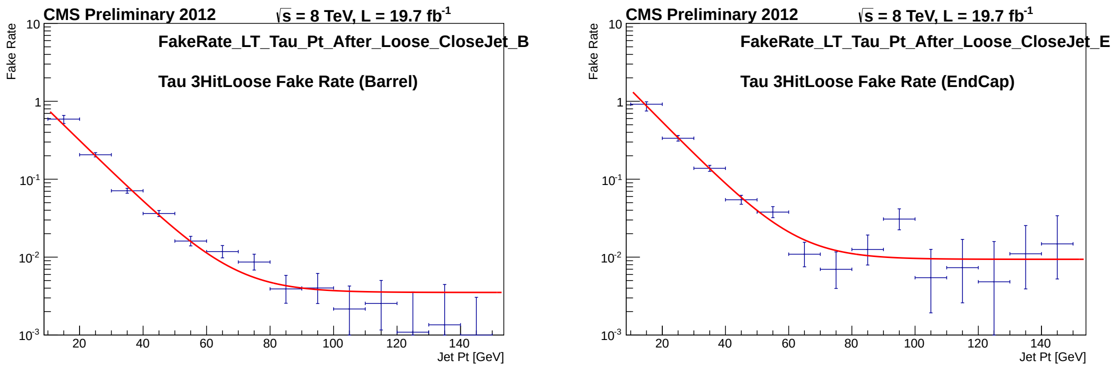

Figure 9: Fit functions for jet $\to \tau_h$ fake rate, in the case the barrel (left) and endcap (right), in $l\tau_h$ final states. The distributions are fitted as a function of the p_T of the jet closest to the reconstructed tau.

6.2.3 Jet $\to \tau_{had}$ fake rate measurement in $ll + l\tau_h$ final states

The hadronic tau fake rate is measured from the $\mu\tau_h$ and $e\tau_h$ channels. The selections are the same as those outlined in Section **??**, with the exception that the tau isolation has not been applied. The fake rate is calculated as the ratio of the number of events that pass all selections to the number of events that pass all selections other than isolation. This fake rate is measured for various bins of closest jet p_T, then fitted with a falling exponential. Two fits are performed, depending on whether the tau is reconstructed in the barrel ($|\eta| < 1.4$) or endcap ($|\eta| > 1.4$) of the detector, see Fig. 10.

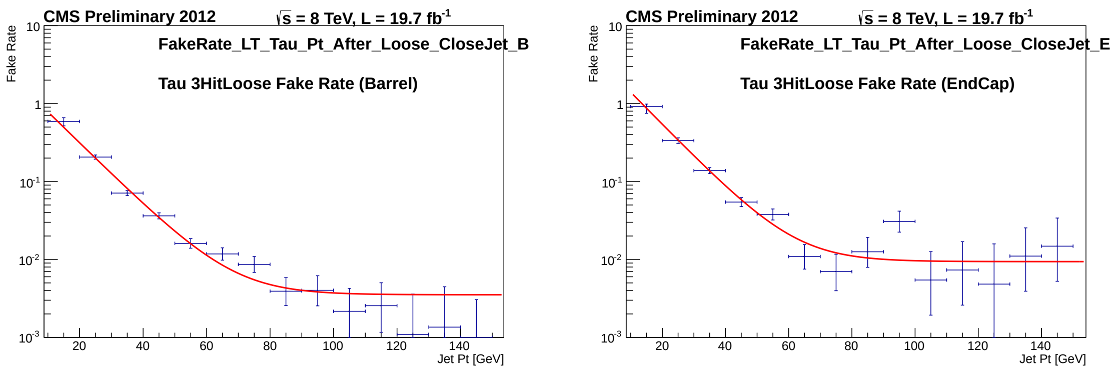

Figure 10: Fit functions for jet $\to \tau_h$ fake rate, in the case the barrel (left) and endcap (right), in $\tau_h\tau_h$ final states. The distributions are fitted as a function of the p_T of the jet closest to the reconstructed tau.

6.2.4 Reducible background normalization

Data events are split into the three following categories and assigned the following weights:

- Category 0. Events that fail isolation or identification requirements on both tau candidate legs. This category is dominated by Z+jets. These events are assigned the weight
$$F(\tau_1)F(\tau_2)/(1-F(\tau_1))(1-F(\tau_2)) \quad (2)$$

- Category 1. Events that fail isolation or identification requirements on the first tau (the higher p_T tau in $\tau\tau$ events, the electron in $e\mu$ events, and the electron (muon) in $e\tau(\mu\tau)$ events) but pass for the second tau. This category includes Z+jets and a part WZ+jets events. These events are assigned the weight
$$F(\tau_1)/(1-F(\tau_1)) \quad (3)$$

- Category 2. Events that pass selections for the first tau but fail isolation or identification for the second tau. This category includes Z+jets and the seond part of WZ+jets events. The events are assigned the weight
$$F(\tau_2)/(1-F(\tau_2)) \quad (4)$$

The reducible background yield is estimated as the weighted sum of categories 1 and 2 with category 0 subtracted. This combination of categories avoids double-counting of events with more than one fake tau. Table 5 shows the contributions to the reducible background from each category split by channel.

channel	Cat0	Cat1	Cat2	1+2-0
mmtt	0.69(15323)	2.16(129)	0.69(177)	2.16±0.25
mmet	1.72(9897)	3.15(129)	2.25(301)	3.67±0.42
mmmt	0.44(2508)	2.26(125)	0.84(46)	2.66±0.33
mmme	0.28(711)	0.88(49)	0.93(42)	1.53±0.28
eett	0.64(14218)	2.25(124)	0.63(179)	2.24±0.25
eemt	0.37(2178)	1.62(104)	0.54(39)	1.80±0.25
eeet	1.58(8937)	1.75(130)	1.89(238)	2.06±0.29
eeem	0.22(565)	0.23(31)	0.72(31)	0.73±0.18

Table 5: Reducible background counts in each channel and category. These contributions are estimated using the data-driven fake rate method detailed above. The right-most column represents the estimated reducible background contribution in each channel.

6.2.5 Reducible background shape

The reducible background shape is obtained from a signal–free region where the tau candidates have the same charge. In order to obtain smooth templates, the isolation and identification conditions on the leptons are relaxed. The requirements in each final state are listed here below:

- $lle\mu$: Loose Muon ID, muon relative isolation < 2.0 (no ID or isolation requirement on the electron except those of the electron candidates used to estimate the electron fake rate);
- $lle\tau_h$: raw MVA2 tau isolation > -0.95, Loose electron ID, relative electron isolation < 0.3;
- $ll\mu\tau_h$: raw MVA2 tau isolation > -0.95, Loose muon ID, relative muon isolation < 0.7;
- $ll\tau_h\tau_h$: raw MVA2 tau isolation > -0.95.

These requirements have been chosen in such a way as to increase the statistics while keeping a constant composition of the reducible background. It has been shown, using a simulated $WZ \to 3l\nu$ MC sample, that the WZ contribution is well included in the reducible background. In particular, the high MET shape of the reducible bacground, coming essentially from WZ+jets events, is well described with these relaxing criteria.

In addition, the LT cut is relaxed to 50 GeV for the fully hadronic final state, whereas it is kept the same as in the final selection for the other final states.

6.2.6 Reducible background shape cross-check

The shape of the reducible background is extracted from a same-sign region with loosened isolation to increase the statistics and obtain a smooth template. It can be shown that, within the uncertainties, the shapes obtained from this signal–free region are compatible with the shapes extracted by weighting the events with non isolated/identified leptons with the fake rate method. Fig. 11 compares the shapes obtained with both techniques in different final states.

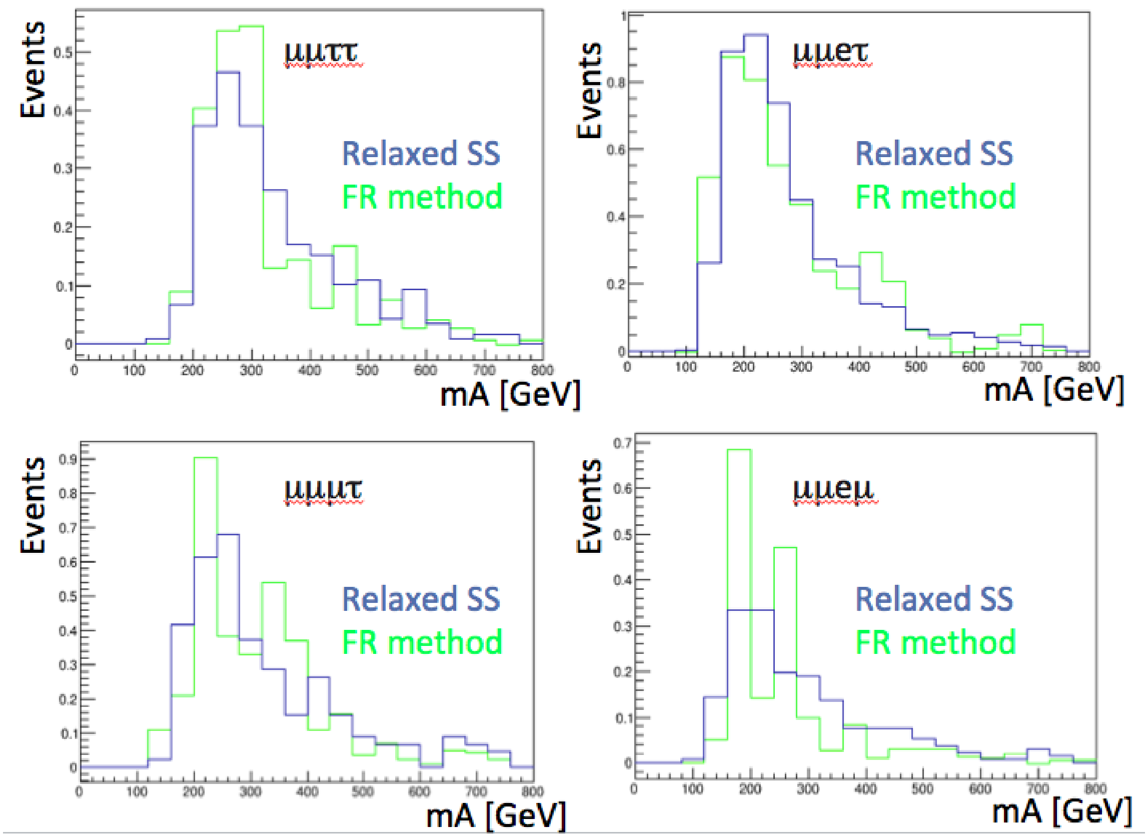

Figure 11: Reducible background shapes obtained with the fake rate method (green) or from the SS relaxed region, in four different final states. Within the uncertainties, both methods give compatible shapes. Because the templates are smoother, the shapes are estimated from a SS relaxed region.

7 Control plots

This section presents some background distributions in control regions.

Fig. 12 shows the mass plots when the selection is the same as in Sec. 5, except that the two taus are required to have the same charge. This region is dominated by reducible background. Within the limited statistics, the data agrees well with the predictions.

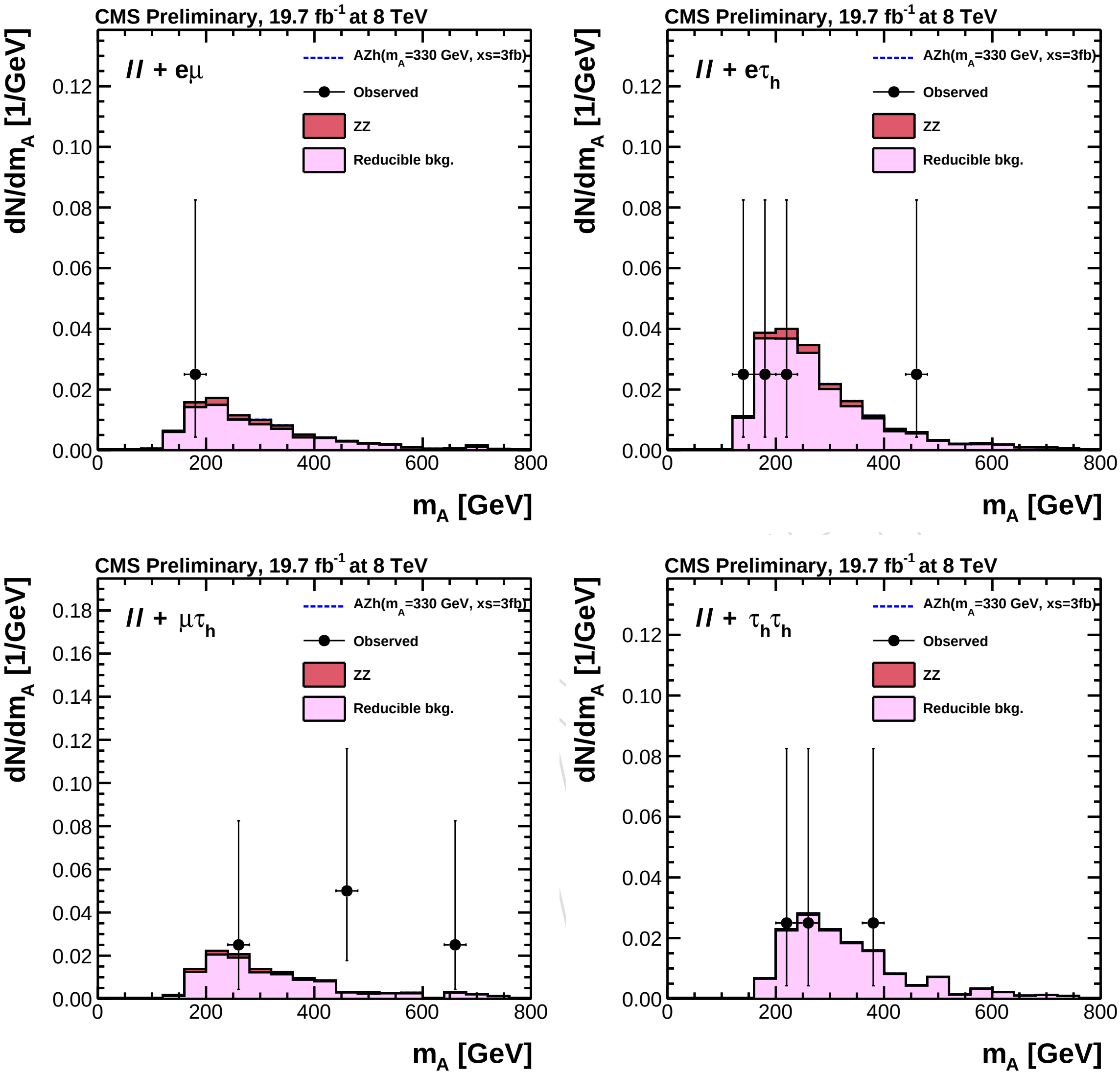

Figure 12: Mass plots when the taus are required to have the same sign, in all considered di-tau final states.

In order to increase the statistics, the previous plots can be reproduced by relaxing some cuts: the L_T cuts are removed in all final states and the tau isolation in $ll\tau_h\tau_h$ final states is relaxed from Medium to Loose. The results are shown in Fig. 13.

A way to check the estimation of the reducible background in the SS region is to relax the tau isolation. A much looser isolation working point is chosen: MVA identification with lifetime information very loose. The prediction from the fake rate method is shown by the blue solid line, while predictions from Monte Carlo, which are very limited statistically, are also illustrated. The fake rate method gives a good agreement with data in $ll\tau_h\tau_h$, whereas the agreement is reasonable in the less populated $lle\tau_h$ final states, see Fig. 14.

The Monte Carlo estimation of ZZ diboson production can be checked in $llee$ and $ll\mu\mu$ events.

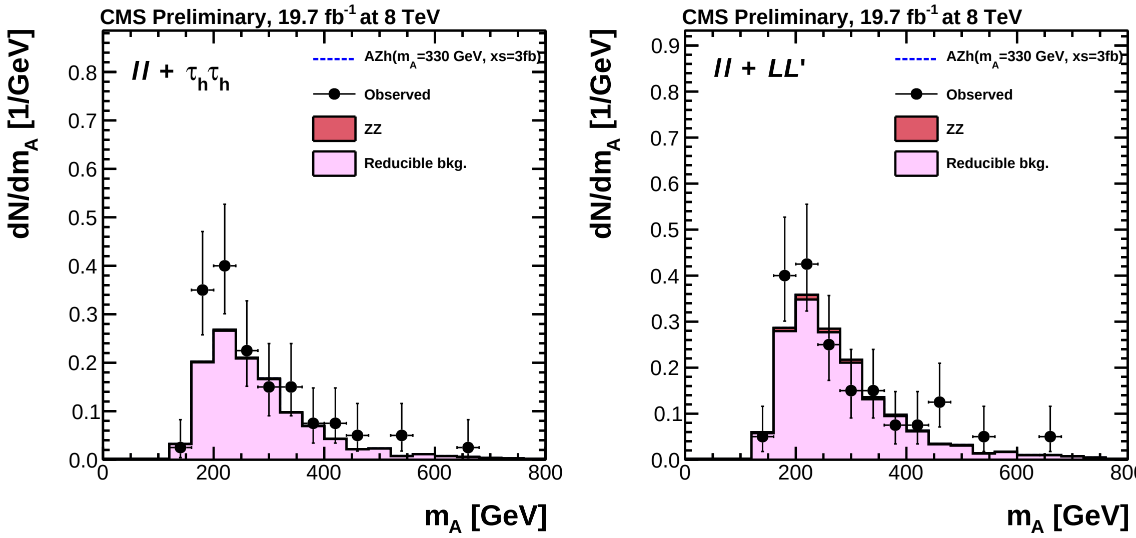

Figure 13: Mass plots when the taus are required to have the same sign, without L_T cut and with loose tau isolation. $ll\tau_h\tau_h$ channels are shown in the left-hand side while all final states combined are shown in the right-hand side.

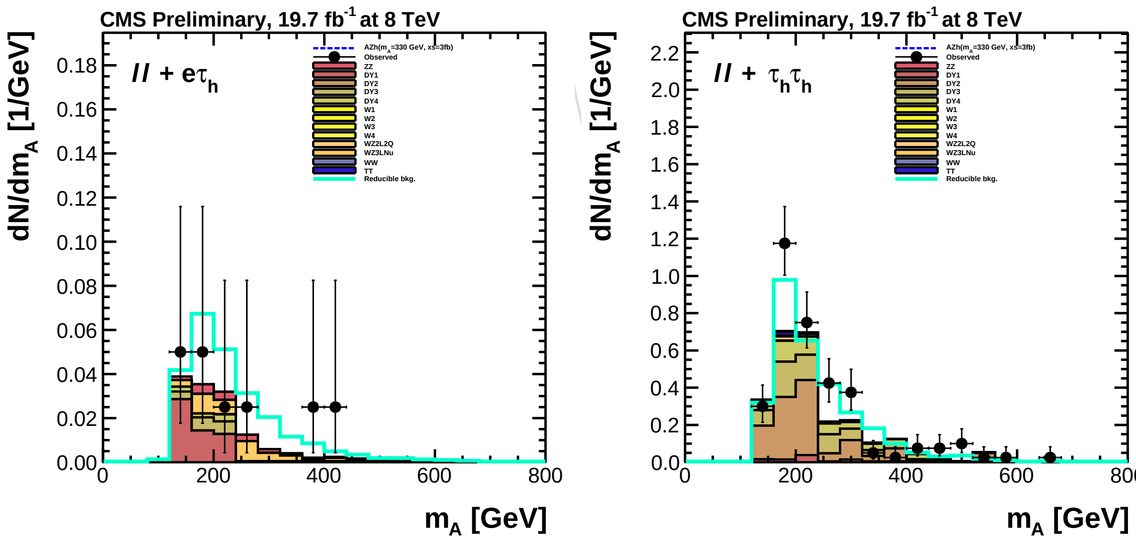

Figure 14: Predictions from the fake rate method (blue line) and from Monte Carlo (filled couloured areas) in a SS region with MVA with lifetime information very Loose isolation for all hadronic taus. The fake rate method agrees well with data in $lle\tau_h$ (left) and $ll\tau_h\tau_h$ (right) final states.

As shown in Fig. 15, the ZZ prediction described data well in those two final states.

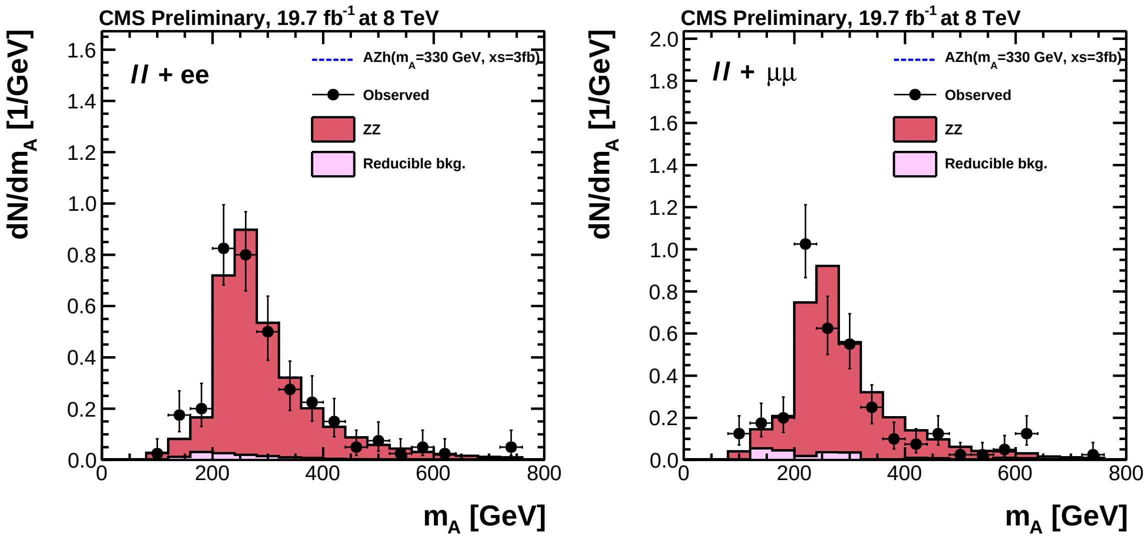

Figure 15: ZZ prediction and observed data in a region with two pairs of opposite sign light leptons.

8 Scale factors and event-by-event weights

8.1 Trigger efficiency

To compensate the difference in trigger efficiency between data and MC, both data and MC trigger efficiencies are fitted with a Crystalball function and the scale factor is obtained by dividing these two functions.

8.2 Lepton identification and isolation efficiency

Scale factors are applied to correct the difference in efficiency between the identification and isolation of electrons and muons between data and MC.

8.3 Pileup reweighting

Simulated events are reweighted to account for the difference in the distribution of reconstructed vertices between data and MC.

9 Systematic uncertainties

The sources of systematic uncertainties that are common for all final states are summarized in the top part of the Table 6. The pp integrated luminosity uncertainty amounts to 2.6% for 2012 [16].

The main uncertainty on the estimation of the ZZ background arises from the theoretical uncertainty on the ZZ production cross section. The results obtained for PDF and QCD scale uncertainties, summarized in the Table 6, are treated as uncorrelated for each production mode considered.

The uncertainty on reducible background is estimated by evaluating an individual uncertainty for each lepton fake rate and applying it to the background calculation.

One part of the uncertainty on the tau fake rate is due to the uncertainty on the fit of the fake rate. As mentioned earlier, the dependency of the fake rate on the associated jet p_T is fitted with an exponential function. The uncertainties on the fitted parameters are used to compute upper and lower bounds for the fitting function. Additionally, it is shown that 20% uncertainty band on tau fake rate, can cover the fit uncertainty as well as statistical fluctuation.

The same procedure is applied for electron and muon fake rates. The presence of an attidional tau in the event leads to a lower rate since it induces a greater hadronic activity in the event. To compensate for the slightly different topologies in which these fake rates are extracted and applied, we assign a 30% uncertainty. This band also covers the fit uncertainty and statistical fluctuations.

The 20% uncertainty on tau fake rate and 30% correlated uncertainty on the electron and muon fake rates are propagated through the background calculation to derive individual systematic uncertainties for each decay channel. By propagating these uncertainties on the fake rate and re-calculating the reducible backgrounds for all eight final states, it can be seen that the total amount of reducible has a total uncertainty between 10 to 30%, depending on the channel. Tau fake rate uncertainty in tautau final states, tau fake rate uncertainty in l-tau final state and electron/muon fake rate in l-tau and ll final states are accounted to be uncorrelated with each other, as they have been measured differently in different control regions. However they are accounted as correlated among all relevant final states.

The muon and electron trigger efficiencies, identification, isolation values are measured from data with tag–and–probe methods.

The hadronic tau identification uncertainty has been determined 6% by CMS using the tag–and–probe type measurement. The energy scale of the hadronic tau is varied within 3% [14]. The hadronic tau energy scale affects the m_A shape distribution and is considered as a shape systematic in the limit calculation.

10 Results

The blinded massplots in different final states are shown in Fig. 16. The background in $ll\tau_h\tau_h$ final states is dominated by the reducible background, while $lle\mu$ final states are dominated by irreducible processes, essentially ZZ diboson production.

Exclusion limits on the cross-section times branching ratio are set at 95% confidence level, using the CLs method [17]. As shown in Fig. 17 and Fig. 18, cross-sections times branching ratio between ... and ... are expected to be excluded for masses between 220 and 350 GeV.

11 Summary

A MVA rejection of ZZ irreducible background

ZZ diboson production is an irreducible background because, as is the case for the signal, it can result in four real leptons in the final state. In the analysis presented here, it is reduced by a cut on the scalar p_{T} sum of the taus originating from the h boson. However there are many more handles that permit to discriminate it from the signal $A \to Zh \to ll\tau\tau$. These

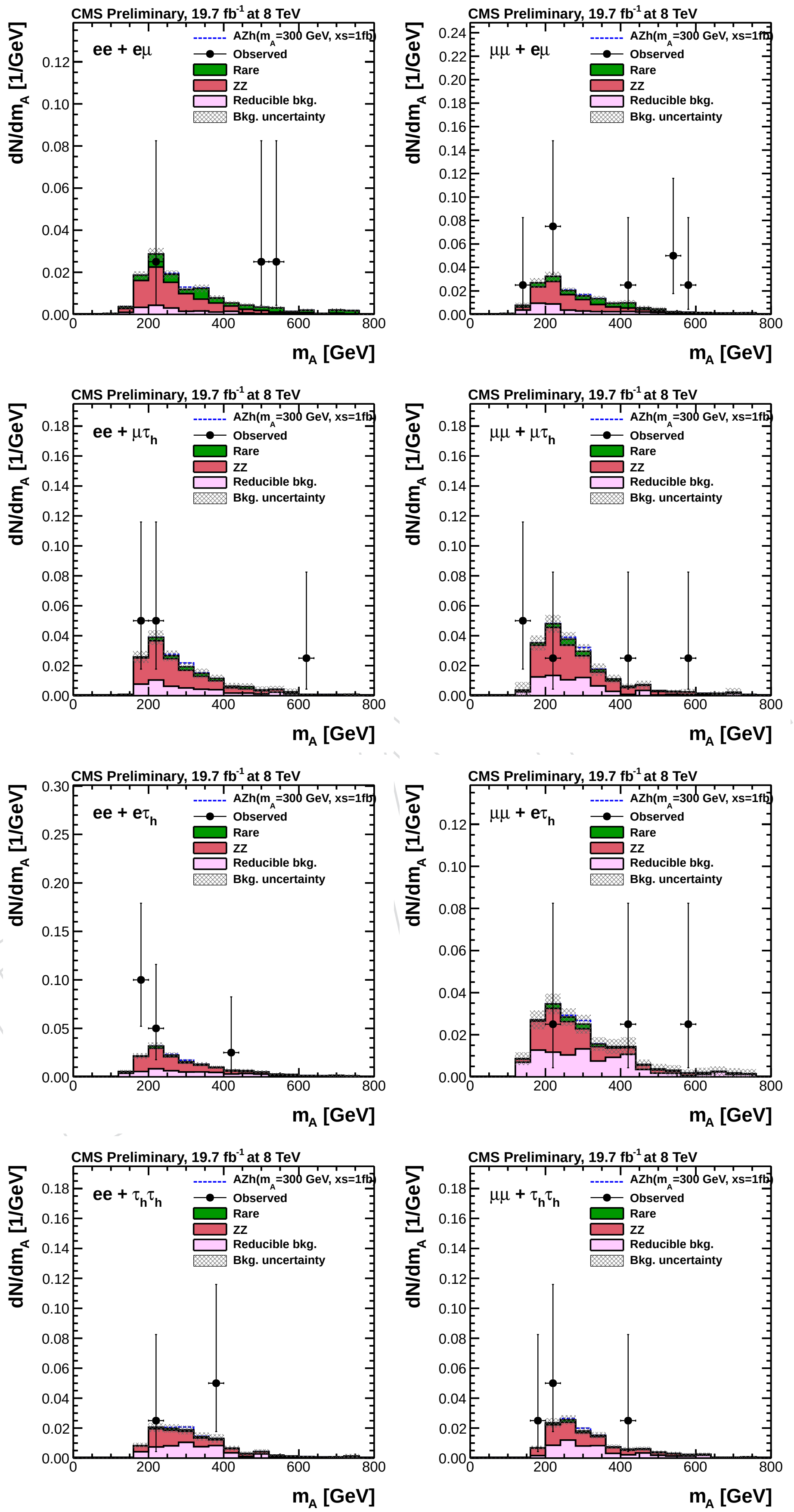

Figure 16: Mass plots, blinded between 280 and 360 GeV.

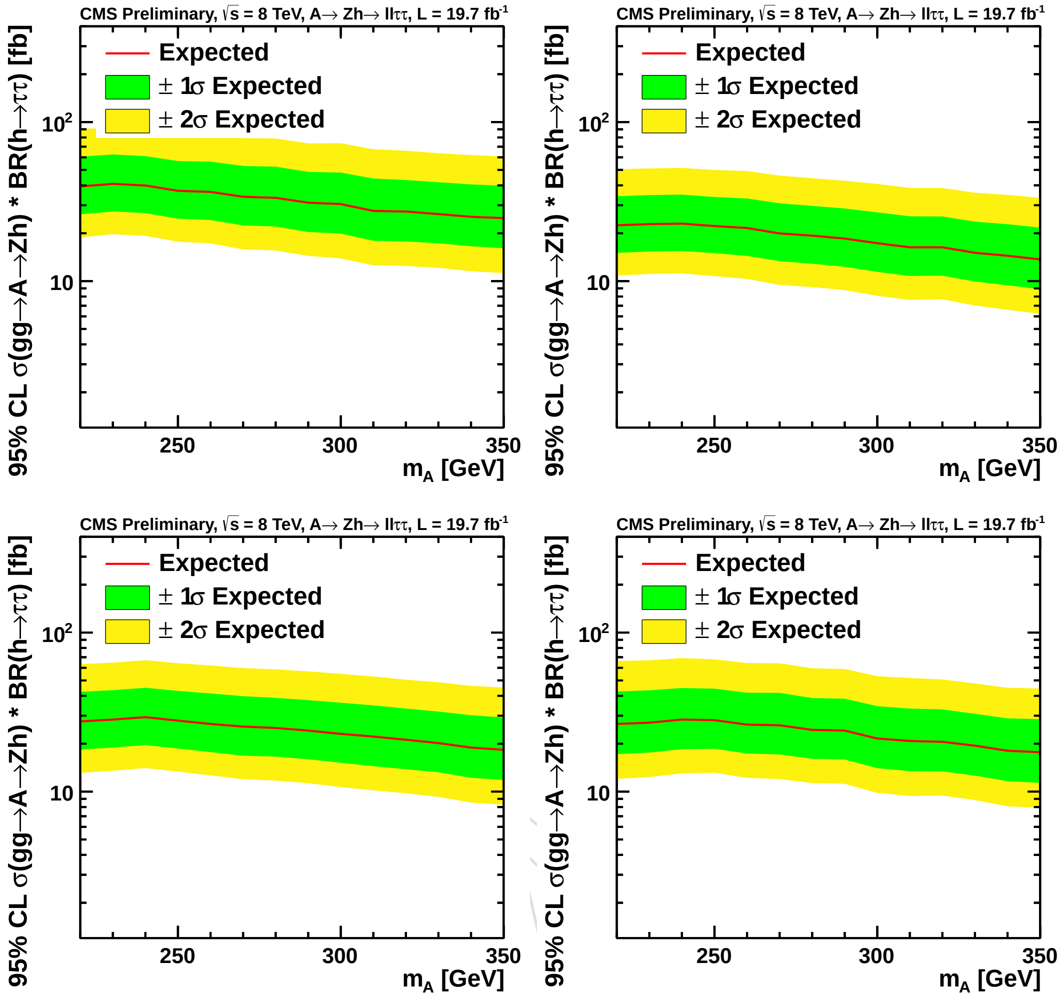

Figure 17: Expected limits in $ll e\mu$, $ll\mu\tau_h$, $lle\tau_h$ and $ll\tau_h\tau_h$ final states.

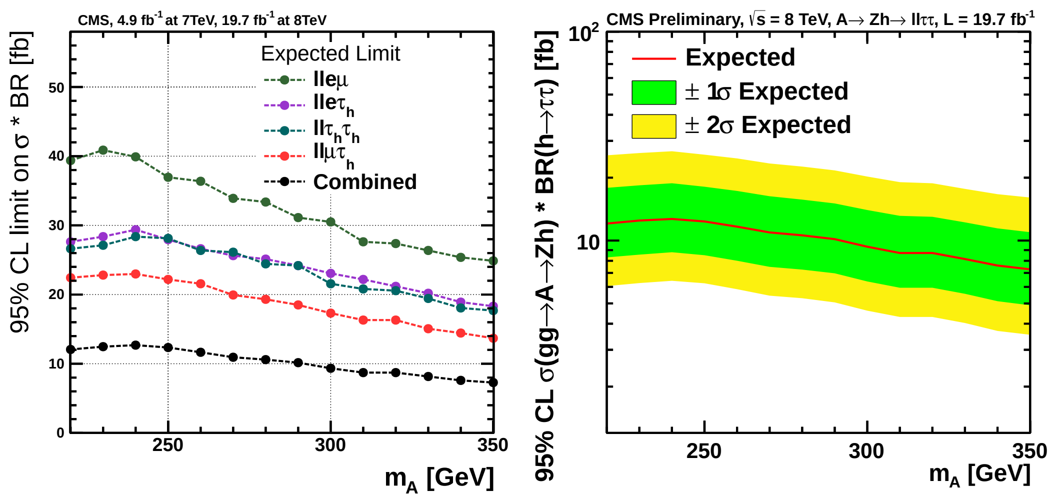

Figure 18: Expected limits in all final states combined, and comparison with the different final states.

Table 6: Systematic uncertainties. The uncertainties on e and μ reconstruction and identification, are isolation are combined; for , the energy-scale uncertainty is reported separately.

Systematic uncertainties common to all channels.	
Source	Uncertainty
Luminosity measurement	2.2-2.6%
Muon trigger efficiency	1%
Muon ID/Iso/ES	2%
Electron trigger efficiency	1%
Electron ID/Iso/ES	2%
Tau ID/Iso	6%(12%)
Tau ES	3%(6%)
Btag	1%
PDF for $q\bar{q} \to ZZ$	5%
PDF for $gg \to ZZ$	10%
QCD scale for $q\bar{q}$	2.6-6.7%
QCD scale for $gg \to ZZ$	24-44%
QCD scale for VHs	2.9%
Reducible background estimate	15-30%
σ_{TTZ}	50%
σ_{WWZ}	50%
σ_{WZZ}	50%
σ_{ZZZ}	50%

discriminating variables may be combined in a Boosted Decision Tree (BDT) to enhance the ZZ/signal discrimination.

Twelve powerful variables have been identified, and are listed here by order of discriminative potential:

- ST, the scalar p_T sum of all four leptons and MET;
- (τ, τ), the distance in the (η, ϕ) plane between the two taus;
- A centrality, the ratio between the vectorial p_T sum of the reconstructed h and Z bosons, and their scalar sum;
- (Z, h), the distance in the (η, ϕ) plane between the reconstructed Z and h boson;
- LT^Z, the scalar p_T sum of the leptons originating from the reconstructed Z boson;
- $\cos\theta_1$, the angle between the negatively charged lepton from the Z and the Z flight direction in the Z rest frame;
- h centrality, the ratio between the vectorial p_T sum of the reconstructed taus, and their scalar sum;
- twist(Z,h), $\Delta\phi(Z, h)/\Delta\eta(Z, h)$;
- h p_T;
- $\cos\theta^*$, the angle between the Z flight direction and the beam axis, in the A rest frame;
- A p_T;
- twist(τ_1, τ_2), $\Delta\phi(\tau_1, \tau_2)/\Delta\eta(\tau_1, \tau_2)$.

The BDT is trained with a mix of signal events with A masses between 290 and 350 GeV. The distributions of the above-mentioned variables are shown in Fig 19 for signal (blue) and ZZ (red). The BDT output distributions as well as the ROC curve are presented in Fig. 20.

Even if cutting on the BDT output has been proven efficient to reduce not only ZZ but also the reducible background, this MVA method has not been used to produce the final results exposed in Sec. 10. The main reason is the lack of statistics in the signal region; the level of control of the backgrouns, especially the reducible one, has not been judged sufficient because of the small number of events. However, the estimated gain of such a method is superior to 20%, and could be used in future runs with larger luminosity.

B $llee$ and $ll\mu\mu$ final states

Six di-tau final states are possible: $\tau_h\tau_h$, $e\tau_h$, $\mu\tau_h$, $e\mu$, ee and $\mu\mu$. The first four have been analyzed in this search for $A \to Zh$. Historically, ee and $\mu\mu$ were not considered in the SM ZH analysis because of the overlap with $H \to 4l$ analysis. The potential of these two channels has been evaluated in the context of A analysis.

Similarly as is the case for $lle\mu$ final states, the contribution from reducible backgrounds is small in $llee$ and $ll\mu\mu$ channels. However ZZ diboson contribution is strongly enhanced because it is impossible to discriminate electrons from Z decays, from electrons from tau decays. A useful handle to reduce the ZZ irreducible background in these final states is the transverse missing energy. Indeed, $ZZ \to llll$ events are not supposed to contain a large MET, whereas four neutrinos are produced in the searched $A \to Zh \to llll$ decay. Fig. 21 illustrates the MET distribution in signal and background events. A threshold of 30 GeV has been chosen for all $llee$ and $ll\mu\mu$ channels, which is a compromise between the signal acceptance at low mass and the ZZ reduction.

The final plots for $llee$ and $ll\mu\mu$ final states are shown in Fig. 22. As expected, the background is dominated by ZZ diboson production, in larger quantities than for $lle\mu$ final states. The corresponding expected limits, compared to the other channels, are presented in Fig. 23, while the improvement in the combined limit obtained by adding the four extra channels is shown in the right-hand side of the same figure. The limits in $llee$ and $ll\mu\mu$ final states are much worse than those of the other channels, especially at low mass, which is due to the MET cut. The general improvement in combined limit is less than 5%, which justifies the fact that these channels have not been treated in the core analysis.

Since the general improvement is anyway small at low mass, a higher MET cut can be applied to enhance the limit at high mass. With a 50 GeV cut, the limit gets up to 10% tighter at high A mass, as shown in Fig. 24.

References

[1] CMS Collaboration Collaboration, "Observation of a new boson at a mass of 125 GeV with the CMS experiment at the LHC", *Phys.Lett.* **B716** (2012) 30–61, doi:10.1016/j.physletb.2012.08.021, arXiv:1207.7235.

[2] H. E. Haber, "Introductory low-energy supersymmetry", arXiv:hep-ph/9306207.

[3] Checcia, P. and others, "Search for new physics in the $A \to Zh \to llbb$ channel", *CMS Note* **2013/302** (2013).

[4] CMS Collaboration Collaboration, "Evidence for the 125 GeV Higgs boson decaying to a pair of τ leptons", arXiv:1401.5041.

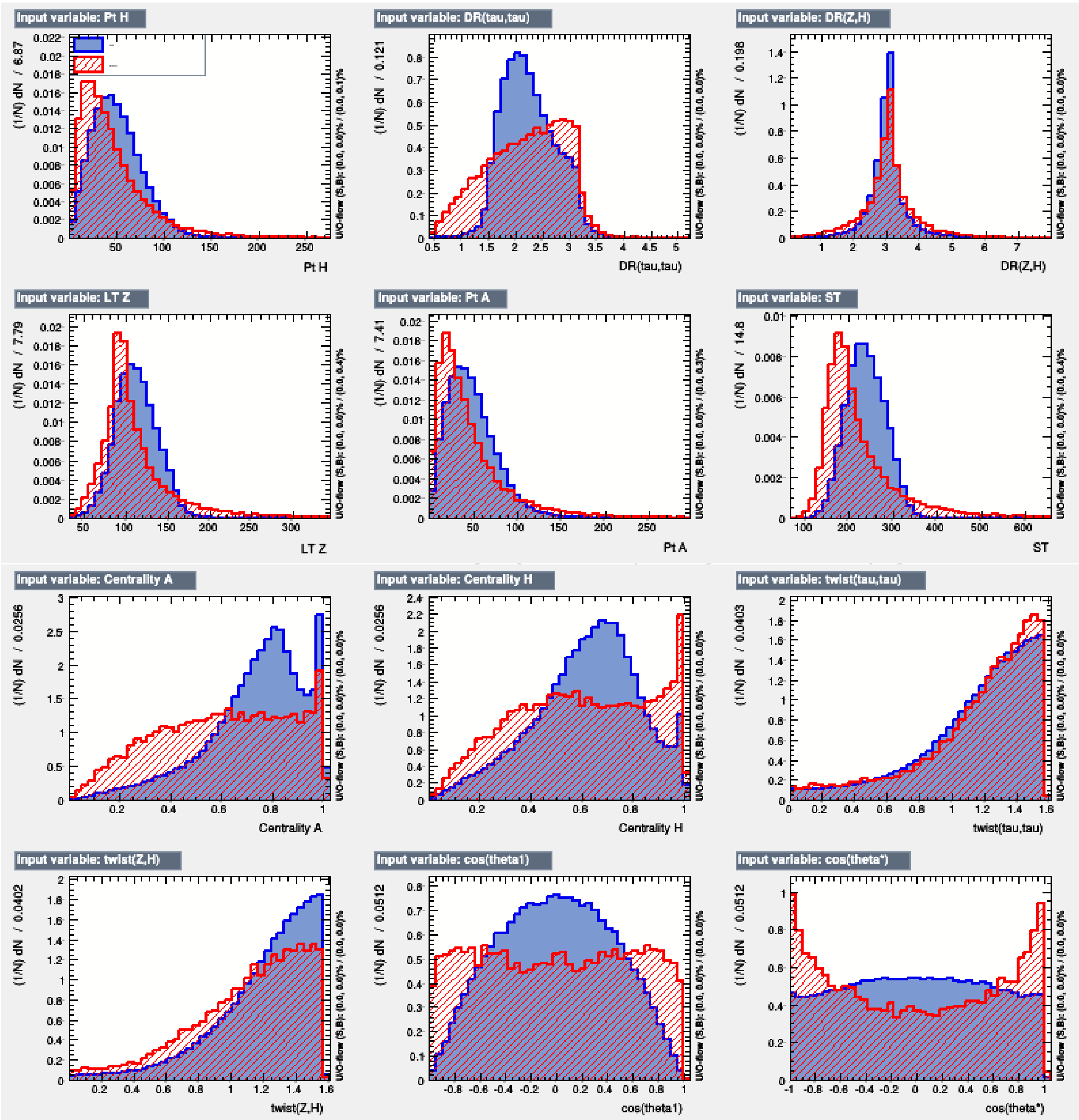

Figure 19: BDT input variables for signal (blue) and ZZ (red) processes.

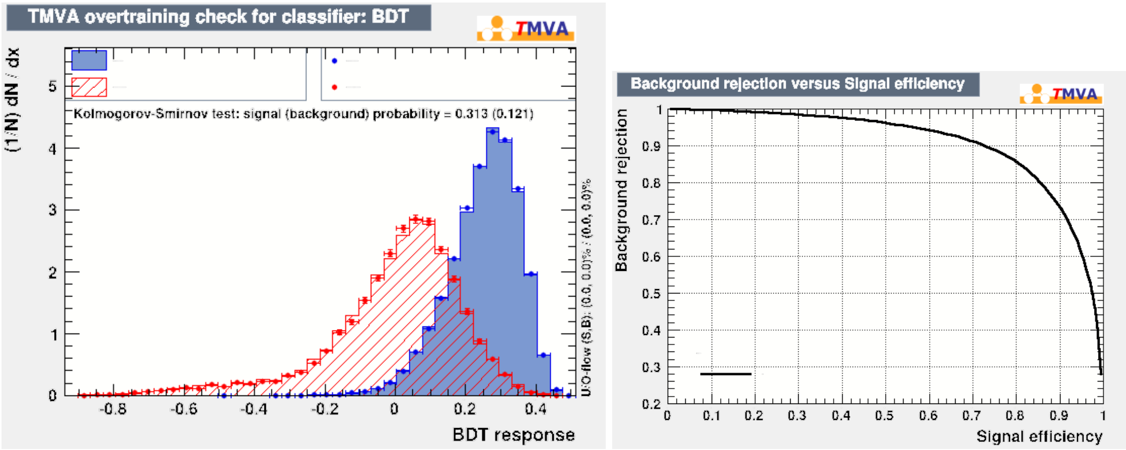

Figure 20: Signal and background distributions of the BDT output (left) and ROC curve (right).

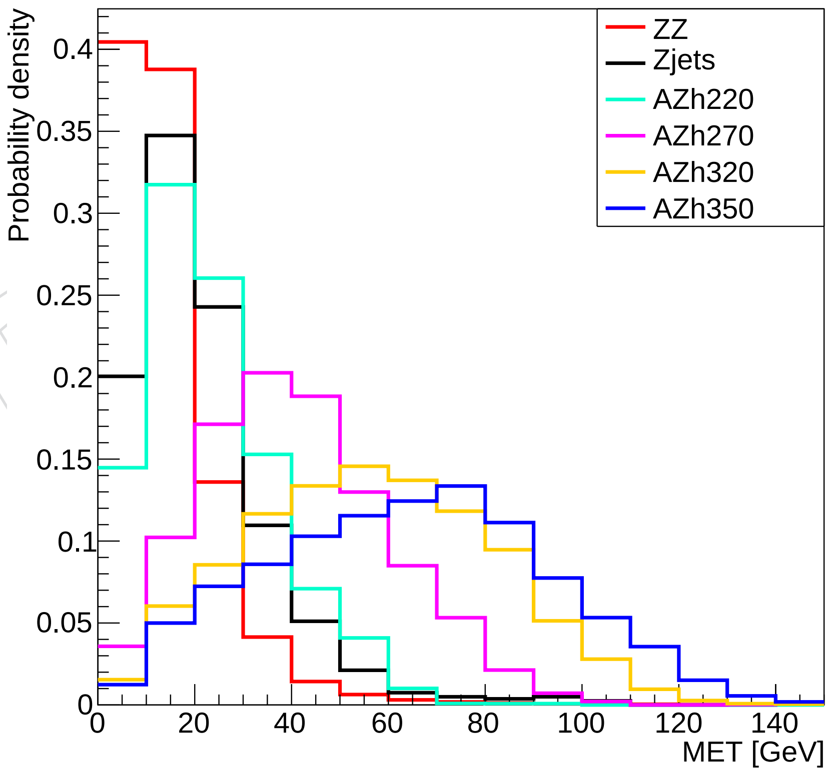

Figure 21: MET distributions for signal at different masses and backgrounds, in the *eeee* final state. A cut on the MET variable may increase the $S/\sqrt{B}$ ratio.

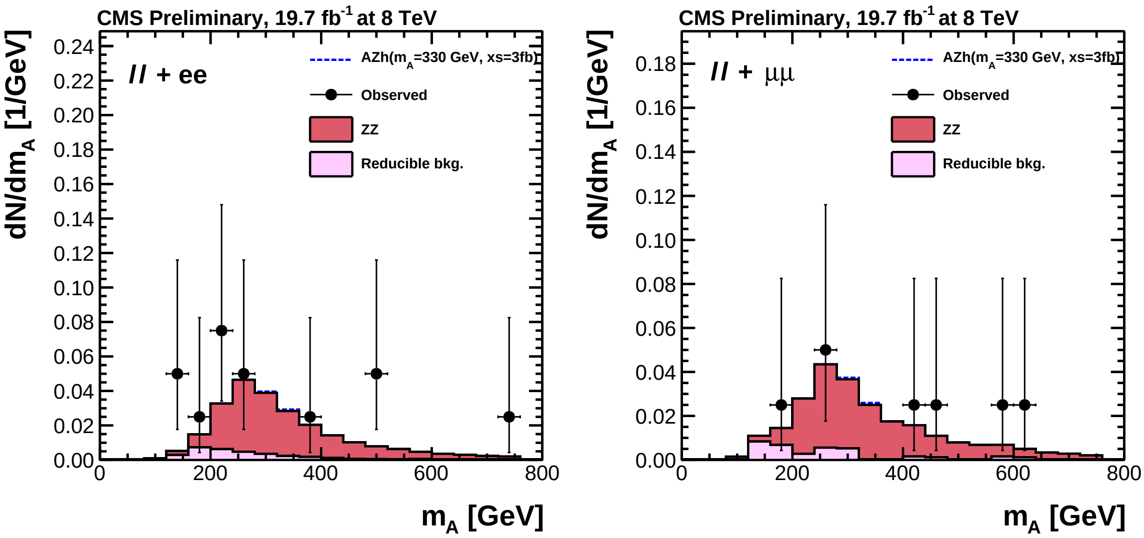

Figure 22: Mass plots in $llee$ and $ll\mu\mu$ final states, blinded between 280 and 360 GeV.

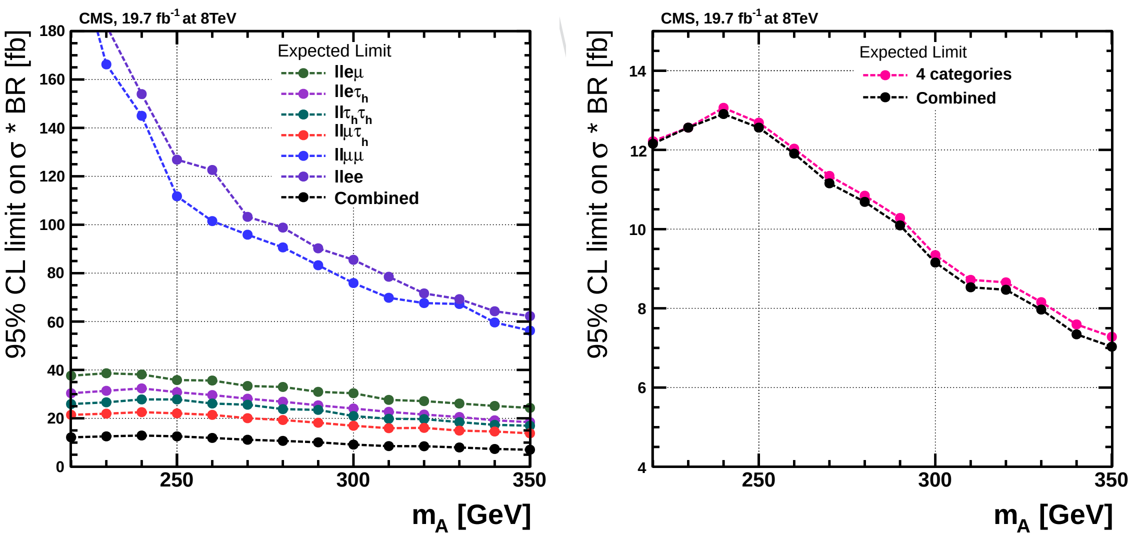

Figure 23: Comparison of expected limits by channel.

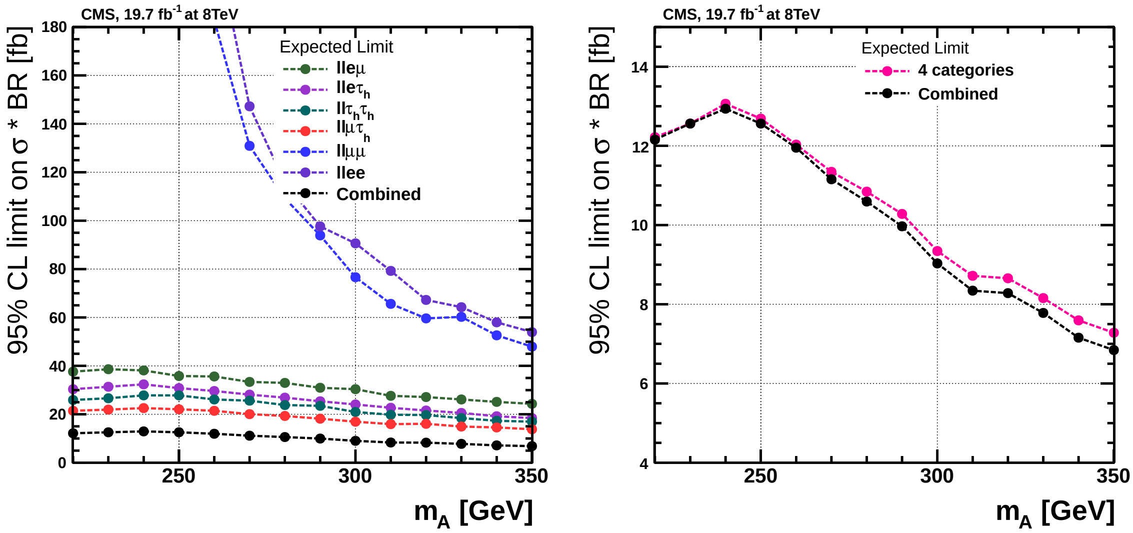

Figure 24: Comparison of expected limits by channel.

[5] J. Alwall et al., "MadGraph 5 : Going Beyond", *JHEP* **1106** (2011) 128, doi:10.1007/JHEP06(2011)128, arXiv:1106.0522.

[6] S. Jadach, Z. Was, R. Decker, and J. H. Kuhn, "The tau decay library TAUOLA: Version 2.4", *Comput.Phys.Commun.* **76** (1993) 361–380, doi:10.1016/0010-4655(93)90061-G.

[7] M. Hildreth et al., "https://twiki.cern.ch/twiki/bin/view/CMS/PdmVPileUpDescription#S10".

[8] M. Hildreth et al., "https://twiki.cern.ch/twiki/bin/viewauth/CMS/PileupInformation".

[9] S. Agostinelli et al., "G4–a simulation toolkit", *Nuclear Instruments and Methods in Physics Research Section A: Accelerators, Spectrometers, Detectors and Associated Equipment* **506** (2003), no. 3, 250 – 303, doi:10.1016/S0168-9002(03)01368-8.

[10] Higgs TauTau group, "Physics Objects in the Higgs to Tau Tau Analysis", *CMS Note* **2013/188** (2013).

[11] A. Hocker et al., "TMVA - Toolkit for Multivariate Data Analysis", *PoS* **ACAT** (2007) 040, arXiv:physics/0703039.

[12] CMS Collaboration Collaboration, "Particle-Flow Event Reconstruction in CMS and Performance for Jets, Taus, and MET", Technical Report CMS-PAS-PFT-09-001, CERN, 2009. Geneva, Apr, 2009.

[13] CMS Collaboration Collaboration, "Performance of muon identification in pp collisions at s**0.5 = 7 TeV", Technical Report CMS-PAS-MUO-10-002, CERN, 2010. Geneva, 2010.

[14] Tau POG, "Performance of tau reconstruction and identification in *pp* collisions at $\sqrt{s} = 8$ TeV", *CMS Note* **2014/008** (2014).

[15] C. Collaboration, "Performance of -lepton reconstruction and identification in CMS", *Journal of Instrumentation* **7** (2012), no. 01, P01001.

[16] CMS Collaboration, "CMS Luminosity Based on Pixel Cluster Counting Summer 2013 Update", *CMS Physics Analysis Summary* **CMS-PAS-LUM-13-001** (2013).

[17] A. L. Read, "Presentation of search results: the CLs technique", *J. Phys. G: Nucl. Part. Phys.* **28** (2002) 2693, doi:10.1088/0954-3899/28/10/313.